Influence of multiple excitation of low lying states and giant resonances on heavy ion inelastic spectra

Y. Blumenfeld
Institut de Physique Nucléaire, 91406 Orsay Cedex, France

Ph. Chomaz
Division de Physique Théorique, Institut de Physique Nucléaire, 91406 Orsay Cedex, France

(Received 9 December 1987)

The inelastic excitation probabilities of ^{40}Ca, ^{90}Zr, and ^{208}Pb impinged upon by ^{40}Ca projectiles at bombarding energies between 10 and 100 MeV/nucleon are calculated in a model in which the excitation amplitudes are evaluated along classical trajectories. The excited states are calculated in the random-phase approximation and the nuclear and Coulomb excitations of both low lying states and giant resonances of the target and projectile are taken into account. A general feature of the calculated spectra for near-grazing impact parameters and bombarding energies above 20 MeV/nucleon is the presence of broad regularly spaced structures mainly due to the excitation of multiphonon states built with $2\hbar\omega$ giant resonances. Cross-section estimates for the inelastic excitations are given.

I. INTRODUCTION

The excitation of collective nuclear states by heavy ion inelastic scattering has attracted much attention in recent years.[1-3] Indeed heavy ion probes should be favorable for the excitation of high-energy or high multipolarity states.[4] Moreover, collective excitations are predicted to be efficient doorways towards energy dissipation and thermalization in heavy ion reactions.[5] The first studies using low-energy ($E \leq 10$ MeV/nucleon) beams gave clear evidence for the excitation of the giant quadrupole resonance[1] whose cross section has been shown to increase strongly with incident energy.[6] A subsequent detailed study of the inelastic spectra revealed the presence of low cross-section structures ranging up to 80 MeV excitation energy.[7,9] The nature of these structures is still controversial. In experiments using light heavy ion beams (i.e., ^{20}Ne), some of the structures have been seen to be related to projectile excitation followed by particle decay.[8] Conversely, in a systematic study of these high-energy structures undertaken for several target nuclei using intermediate energy ^{40}Ar beams,[10] the excitation energies of the bumps were found to be well reproduced by phenomenological laws of the type $E^* \propto A_T^{-1/3}$, where A_T is the target mass. These observations are compatible with an interpretation of the structures in terms of excitations of collective modes of the target. In light of these experiments two questions must be addressed: Do collective nuclear excitations contribute to the high-energy part of the inelastic spectra and if so can they be responsible for the relatively narrow structures observed experimentally?

The excitation of collective states in heavy ion reactions has been investigated from a theoretical point of view by several methods.[5,9,11-19] Recently it was proposed by the authors in Refs. 9, 16, 17, and 19 that multiphonon excitation can generate structures at high energy. However, in other calculations very low multiphonon excitation probabilities were found.[18,20] In all these approaches the nuclei are assumed to follow classical trajectories but the treatment of the nuclear excitations differs. The Copenhagen model[15,18,20,21] treats these excitations classically and it was shown that the excitation probabilities of giant resonances are too weak to generate multiphonon structures in the inelastic spectra.[18] Conversely, when the excited states are calculated in the random-phase approximation (RPA) it was found that the excitation of $2\hbar\omega$ isoscalar giant resonances is sufficiently important to lead to multiphonon bumps in the inelastic cross section.[9,16,17,19] However, in the latter calculations low-lying states were not included in the response function and the Coulomb interaction was not taken into account. It has been claimed that the inclusion of these points would wash out the observed structures as in the Copenhagen case.[18]

In this paper we present calculations of the inelastic excitation probabilities of several nuclei impinged upon by ^{40}Ca projectiles at various incident energies. The excited states are calculated in the RPA and both low lying states and giant resonances are taken into account. Nuclear and Coulomb excitation of the target and the projectile are calculated. In Sec. II we briefly review the hypothesis and results of the model. Section III is devoted to a study of the properties of multiphonon excitations as a function of target mass, bombarding energy, and impact parameter. Cross-section estimations are also given. In Sec. IV conclusions are drawn.

II. THE MODEL

In this section we briefly outline the multiphonon model described in detail in Refs. 16, 19, 22, and 23. This model is analogous to the classical model of Copenhagen except for the microscopic treatment of the nuclear exci-

tations. A complete comparison of the two models can be found in Ref. 24.

In the model discussed here, the calculation of the inelastic excitations is performed in two steps. The first step consists of the microscopic description of the target and projectile responses to the external field created by their respective partners. The excitation modes are obtained using the RPA and are considered as bosons noted λ.

In the second step a classical calculation of the reaction dynamics is performed. For a given trajectory $R(t)$ associated with an entrance channel angular momentum l, the mean number $\bar{n}^{\alpha}_{\lambda}(l)$ of phonons of type λ in the nucleus α excited by the nucleus β is obtained through

$$\bar{n}^{\alpha}_{\lambda}(l)=|A^{\alpha}_{\lambda}(l)|^2=\left|h^{-1}\int_{-\infty}^{+\infty}e^{i\omega^{\alpha}_{\lambda}t}\langle\lambda_{\alpha}|V^{\beta}(r-R(t))|0_{\alpha}\rangle dt\right|^2 \quad (\beta\neq\alpha)\ , \tag{1}$$

where $\hbar\omega^{\alpha}_{\lambda}$ is the excitation energy of the phonon λ. In Eq. (1)

$$\langle\lambda_{\alpha}|V^{\beta}(r-R(t))|0_{\alpha}\rangle$$

is the RPA matrix element of the one-body mean field V^{β} created by the nucleus β traveling on the classical trajectory $R(t)$ calculated between the ground state $|0_{\alpha}\rangle$ and the one-phonon state $|\lambda_{\alpha}\rangle$ of the nucleus α.

The probability $P^{\alpha}_{\lambda}(l,n)$ of exciting n phonons of type λ in the nucleus α is given by the Poisson distribution:

$$P^{\alpha}_{\lambda}(l,n)=\left[\bar{n}^{\alpha}_{\lambda}(l)\right]^n\exp\left[-\bar{n}^{\alpha}_{\lambda}(l)\right]/n!\ . \tag{2}$$

In order to extend the present formalism to the case of a continuous RPA spectrum we introduce the average phonon number density

$$N(E,l)=\sum_{\lambda\alpha}\bar{n}^{\alpha}_{\lambda}(l)\delta(E-\hbar\omega^{\alpha}_{\lambda})\ , \tag{3}$$

and we obtain the excitation probability distribution of the n-phonon states

$$P_{\rm ex}(E,n,l)=\frac{1}{n!}\mathcal{N}\int N(E_1,l),\ldots,N(E_n,l)\delta(E-E_1,\ldots,-E_n)dE_1,\ldots,dE_n \tag{4}$$

with

$$\mathcal{N}=\exp\left[-\int N(E,l)dE\right]\ . \tag{5}$$

The total excitation probability distribution then reads

$$P_{\rm ex}(E,l)=\sum_n P_{\rm ex}(E,n,l)\ . \tag{6}$$

It must be noted that $P_{\rm ex}(E,l)$ does not correspond to the measured inelastic excitation probability. Indeed since the projectiles are detected after particle decay unbound projectile states must not be included in the convolution (4). Thus $P_{\rm ex}(E,n,l)$ must be replaced by $P(E,n,l)$

$$P(E,n,l)=\frac{1}{n!}\mathcal{N}\int N(E_1,l),\ldots,N(E_n,l)\delta(E-E_1,\ldots,-E_n)H(B^p-E^p)dE_1,\ldots,dE_n\ , \tag{7}$$

where E^p is the total excitation energy in the projectile, B^p is the particle emission threshold of the projectile, and H is the Heavyside function. The excitation probability distribution in the inelastic spectrum is then given by

$$P(E,l)=\sum_n P(E,n,l)\ . \tag{8}$$

III. RESULTS

Using the model described in Sec. II we will discuss the excitation of giant resonances and multiphonon states in inelastic heavy ion collisions.

A. Numerical details

In Ref. 19 the comparison of the excitation of high-lying particle-hole and giant resonance states with the multiphonon states shows that, under grazing conditions and for intermediate incident energies, multiphonons built on $2\hbar\omega$ target resonances dominate the inelastic spectrum and give rise to regularly spaced structures.

In this article we perform a complete calculation of collective state excitations both in the projectile and target nuclei for several heavy ion reactions: Ca+Ca, Ca+Zr, and Ca+Pb. In these calculations Coulomb excitation and the influence of low lying states are included. We have used the RPA results of Ref. 25 which were ob-

tained by a self-consistent HF-RPA calculation with the Gogny force $D1$. For high-energy states with a large Landau spreading we have summed the different components and introduced the corresponding width Γ_L. Except for the Landau spreading Γ_L the $D1$ RPA calculations do not yield the widths of the states. These escape $\Gamma\uparrow$ and spreading widths $\Gamma\downarrow$ were introduced in a phenomenological way by replacing the δ function in formula (3) by a Gaussian function with a total width $\Gamma=\Gamma_L+\Gamma\uparrow+\Gamma\downarrow$. The parameter Γ was taken as the experimental width. When such data is not available reasonable widths were postulated (see Table I). We have tested that important modifications of these width parameters of high-lying states do not affect the final results except if very narrow ($\Gamma\approx 5-6$ MeV) widths are chosen for the very high-energy states. In this case these states could generate structures in the inelastic cross section but, since neither theoretical reasons nor experimental observations support this small width hypothesis, this case will not be further discussed in the following.

It should also be noted that the Doppler broadening due to γ decay of excited projectile states was added to the width of projectile low lying states (see the Appendix).

Table I gives the energy, width, spin, and parity of the RPA states used in the calculation together with the various exhausted percentages of the energy weighted sum rule (EWSR) for the $r^L Y_{L,0}(\theta,\varphi)$ excitation operator. As discussed in Refs. 9, 13, 14, and 19, in a microscopic calculation the response to the operator $r^L Y_{L,0}(\theta,\varphi)$ is not sufficient to define the excitation probabilities of the RPA states but either the complete response to the continuous basis of $j_L(qr)\ Y_{L,0}(\theta,\varphi)$ or the form factor associated with the considered process are necessary. Figure 1 presents an example of the response of ^{40}Ca to $j_2(qr)$ for q between 0 and 1.2 fm^{-1} which illustrates the strong influence of the shape of the excitation operator (see also Refs. 13 and 14). This emphasizes the need of a complete microscopic description of the states and partly explains the differences of the present calculation with the classical calculation of Ref. 18. As discussed in Ref. 24 strong discrepancies exist between microscopic and macroscopic form factors. The microscopic form factors used here were obtained with a Woods Saxon potential for the nuclear part of V:

$$V^N(r)=V_0\Big/\left[1+\exp\left[\frac{r-R_0}{a}\right]\right] \tag{9}$$

with the parameter values

$$\begin{aligned} V_0&=-55\ \text{MeV}\ ,\\ a&=0.55\ \text{fm}\ ,\\ R_0&=1.3A^{-1/3}\ \text{fm}\ , \end{aligned} \tag{10}$$

and a point-charge potential for the Coulomb part.

The relative motion $R(t)$ was calculated by solving the classical equation of motion with an ion-ion potential obtained by folding the target Hartree-Fock (HF) density with the projectile mean field renormalizing by a factor

TABLE I. RPA response functions for the three nuclei considered in the calculations. The widths of the states are determined as explained in the text.

Nucleus	J^π	E (MeV)	% EWSR	Γ (MeV)
Ca	0^+	20.00		5.0
	2^+	17.88	98.9	4.0
	3^-	3.56	18.6	
	3^-	9.77	13.1	3.0
	3^-	32.99	67.3	8.0
	4^+	17.56	48.5	4.0
	4^+	41.00	48.0	10.0
Zr	0^+	18.53		3.5
	1^-	31.00		10
	2^+	5.36	8.9	
	2^+	15.77	77.9	3.5
	2^+	46.50	0.1	15
	3^-	2.59	10.5	
	3^-	7.86	23.9	2.0
	3^-	29.95	51.4	10.0
	4^+	5.82	3.6	
	4^+	7.93	5.0	2.0
	4^+	14.80	17.8	4.0
	4^+	44.00	40	15.0
	5^-	1.75	0.6	
Pb	0^+	14.63		3.5
	2^+	5.19	14.4	
	2^+	12.74	60.8	3.0
	2^+	39.18	16.7	15.0
	3^-	3.68	22.0	
	3^-	24.25	33.7	10
	4^+	5.69	6.8	
	4^+	9.56	6.4	2.5
	4^+	15.24	13.2	3.5
	4^+	35.44	17.3	15.0
	5^-	4.56	3.3	
	5^-	19.16	7.9	8.0
	5^-	26.00	15.5	12.0
	5^-	46.54	3.4	20.0

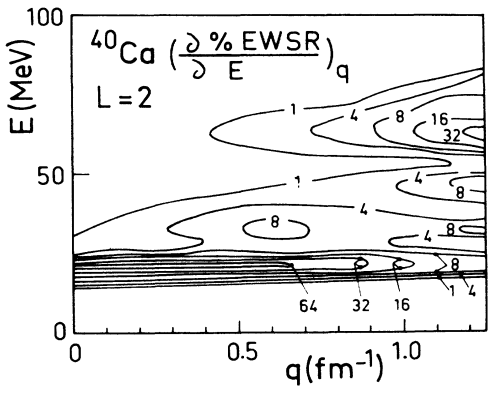

FIG. 1. Bidimensional contour plot of the $L=2$ response of ^{40}Ca to the $j_L(qr)$ operator as a function of momentum transfer q and of excitation energy E. The RPA calculations are from Ref. 14.

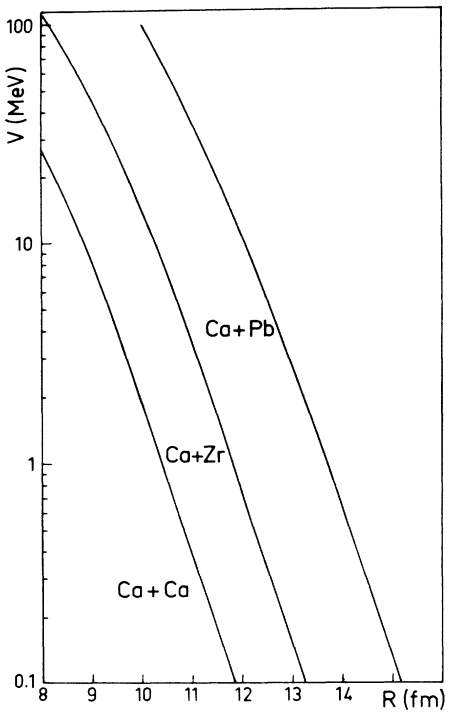

FIG. 2. Real nucleus-nucleus potentials obtained by the convolution method (see text) for the three reactions studied as a function of relative distance R.

0.5 according to the prescription of Satchler[26] in order to simulate the effects of the Pauli principle between nucleons of the two nuclei. Figure 2 shows the nucleus-nucleus potentials used for the three reactions studied. We have tested that the same potentials are obtained when the projectile HF density is folded with the target mean field. Figure 3(a) shows the three deflection functions for the three reactions at 33 MeV/nucleon and Fig. 3(b) the distance of closest approach associated with each trajectory.

Using the model described in Sec. II, we can compute the function $\bar{n}^{\alpha}_{\lambda}(l)$ or $\bar{n}^{\alpha}_{\lambda}(\theta)$, where l and θ are, respectively, the entrance channel angular momentum and the classical deflection angle associated with the same trajectory. In Fig. 4(a) the influence of the parameters R_0, a, and V_0 which are the only parameters of the model are tested. For a given l, the different mean numbers of excited phonons are seen to be sensitive to a variation of the parameters, but on the contrary, the $\bar{n}(\theta)$ function is very stable especially when the variations of the grazing angle as a function of the potential are corrected [Fig. 4(b)]. This reflects a cancellation of the variations of $\bar{n}(l)$ and of $\theta(l)$ which are computed with the same nucleon-nucleus potential. In conclusion the following results presented as a function of θ can be considered as parameter independent.

B. The Ca+Ca reaction at 1320 MeV

First let us consider the Ca+Ca reaction at 1320 MeV as a typical case. We have computed the mean numbers of excited phonons $\bar{n}$ for several trajectories near the grazing. Table II gives for $l=225\hbar$ this mean number of excited phonons $\bar{n}$ for all the considered states. The nuclear ($\bar{n}_n$) and Coulomb ($\bar{n}_c$) contributions are also explicitly given. This table illustrates the strong nuclear excitation and the importance of low lying states. Since this reaction is symmetric the excitation of the target and the projectile are equal. Therefore the projectile excitation is strong and cannot be neglected. However one must discuss the $P(E)$ function [Eq. (7)] which is comparable to the experimental inelastic spectrum. Four $P(E)$ distributions associated with four different angular mo-

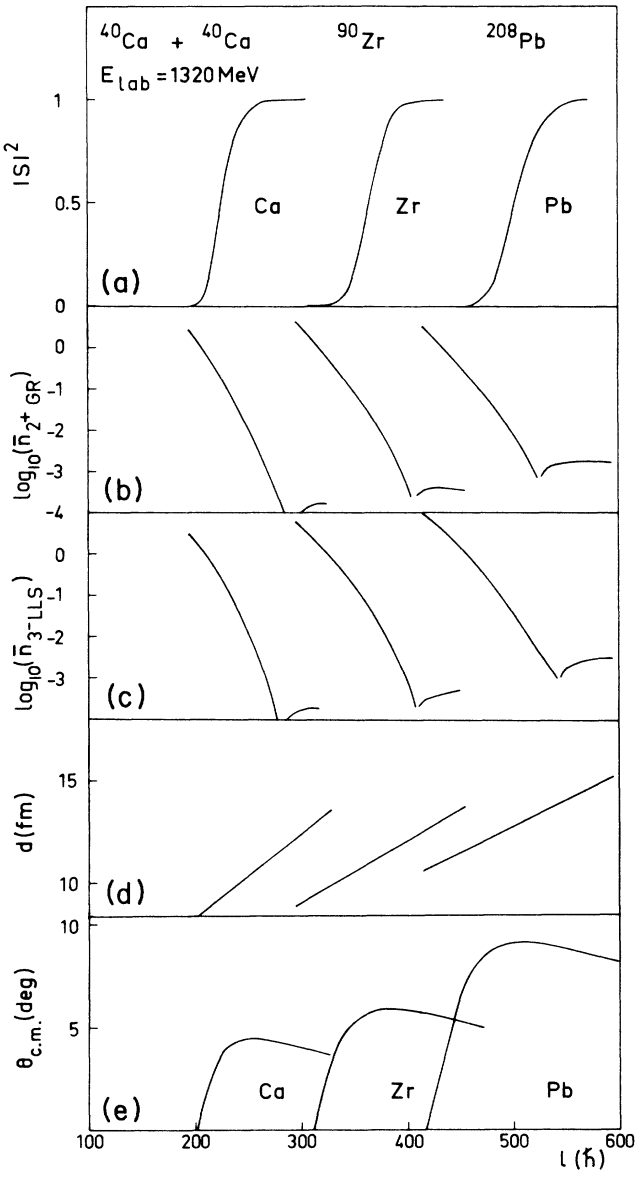

FIG. 3. For the three reactions studied at $E_{\rm lab}=33$ MeV/nucleon as a function of entrance channel angular momentum l (a) deflection function; (b) distances of closest approach; (c) mean numbers of excited phonons for the giant 2^+ state; (d) mean numbers of excited phonons for the low-lying 3^- state; (e) $\mathcal{N}$ [see Eq. (13)].

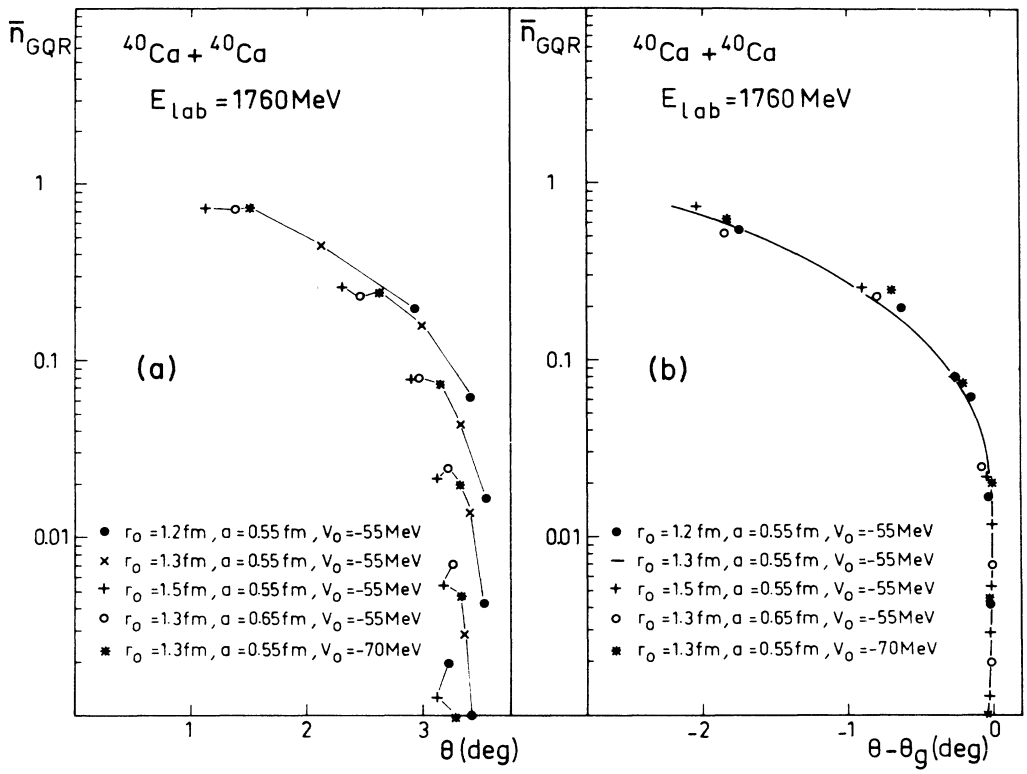

FIG. 4. Mean numbers of excited phonons for the giant quadrupole resonance in the Ca+Ca reaction at $E_{lab} = 44$ MeV/nucleon for different nucleon nucleus potentials. (a) As a function of deflection angle θ. The solid lines join the points corresponding to a fixed distance of closest approach. (b) As a function of the deflection angle rescaled to take into account the variations of the grazing angle for the different potentials.

menta l (or four deflection angles θ), are displayed in Fig. 5. The monophonon distributions $P(E,l)$ are also given for comparison. One can notice the strong angular evolution of $P(E)$. For large angular momenta the spectrum is determined by the Coulomb and nuclear excitation of the monophonon component, whereas for grazing and subgrazing trajectories the nuclear excitation of multiphonons becomes dominant. Moreover, this multiphonon component exhibits broad regularly spaced structures.

To understand these structures we present in Figs. 6 and 7 two different decompositions of the $l = 225\hbar$ spectrum. Figure 6 shows the contribution of the excitations of the target to the total spectrum. As expected the target excitations account for only half of the total excitation of low lying states but the contribution of projectile states is broadened due to the Doppler shift induced by γ decay before detection. For the high lying part of the spectrum the influence of the projectile is very small. This fact is related to the cut at B^p in Eq. (7) which reflects the particle decay of projectile before detection. In addition, the Doppler width smoothes the contribution of projectile excitation in the high excitation region. In conclusion, the mutual excitation of the two partners is important but its influence on the inelastic spectrum is small.

It must however be noted that transfer evaporation reactions, in which the projectile picks up a nucleon from

TABLE II. Total mean numbers of excited phonons and mean numbers of phonons excited by nuclear and Coulomb potentials for the various RPA states in the Ca+Ca reaction at $E_{lab} = 33$ MeV/nucleon and $l = 225\hbar$.

Nucleus	J^π	E (MeV)	$\bar{n}$	$\bar{n}_n$	$\bar{n}_c$
Ca	0^+	20.00	0.42×10^{-1}	0.42×10^{-1}	
	2^+	17.88	0.19	0.24	0.27×10^{-2}
	3^-	3.56	0.24	0.28	0.16×10^{-2}
	3^-	9.77	0.78×10^{-1}	0.89×10^{-1}	0.48×10^{-3}
	3^-	32.99	0.28×10^{-1}	0.30×10^{-1}	0.24×10^{-4}
	4^+	17.56	0.77×10^{-1}	0.83×10^{-1}	0.12×10^{-3}
	4^+	41.00	0.45×10^{-2}	0.46×10^{-2}	0.18×10^{-5}

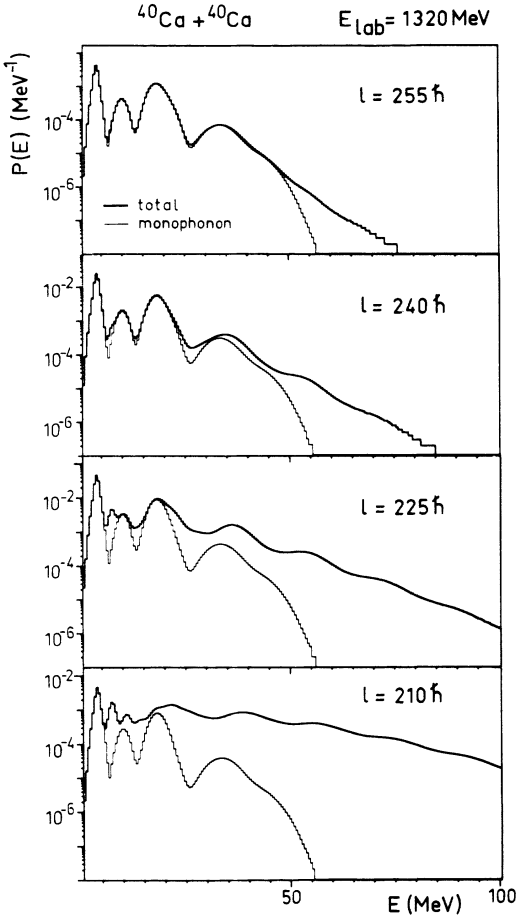

FIG. 5. Inelastic excitation probability spectra for the $^{40}Ca+^{40}Ca$ reaction at $E_{lab}=33$ MeV/nucleon for our different entrance channel angular momenta. The thick lines represent the total excitation probabilities and the thin lines the monophonon probabilities.

the target and subsequently decays by particle emission are not taken into account in these calculations but can contribute to the experimental inelastic spectra (for more details see Ref. 27).

Figure 7 shows a decomposition of the same spectrum into the various multiphonon components. One can see that the situation is quite complex. However, the first multiphonon bump around 36 MeV excitation energy can

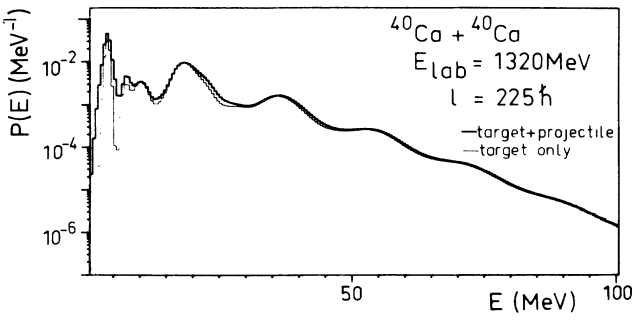

FIG. 6. Thick line: total excitation probability spectrum for the Ca+Ca reaction at $E_{lab}=33$ MeV/nucleon and $l=225\hbar$. Thin line: target excitation probability for the same reaction.

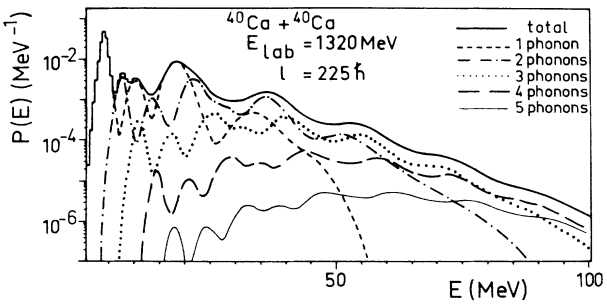

FIG. 7. Decomposition of the inelastic excitation probability (thick line) for the $^{40}Ca+^{40}Ca$ reaction at $E_{lab}=33$ MeV/nucleon and $l=225\hbar$ into components corresponding to different numbers of excited phonons (other lines).

be mainly related to a two $2\hbar\omega$ phonon state. The other structures correspond to various mixings of multiphonon states but always contain a large component of $2\hbar\omega$ phonons and are roughly located at excitation energies multiples of the GQR energy.

This discussion qualitatively confirms the results of the previous calculations[9,16,17,19] which did not include low lying states and projectile excitations. However from a quantitative point of view these two effects are very important. (We have also tested that the results we present and those of Refs. 9, 17, and 19 exhibit a deviation of less than 10% for the mean numbers of phonons of the giant resonance excitations.)

In conclusion, this calculation shows that the presence of high lying structures due to $2\hbar\omega$ giant resonance multiphonon excitations must be expected in inelastic heavy ion spectra.

C. Energy and target dependence

Figure 8 shows five inelastic Ca+Ca spectra at five different incident energies computed for a grazing trajectory defined by a distance of closest approach $d=9$ fm. On this figure three different regimes can be distinguished. At high incident energy ($E>100$ MeV/nucleon) a strong high-energy monophonon contribution is present. In the intermediate-energy region this contribution is weakened and progressively replaced by multiphonon excitations. At low incident energy neither giant resonance nor multiphonon excitations are visible. This fact is related to the strong excitation of low lying states compared to giant resonances and will be discussed in Sec. III D.

Figure 9 presents three inelastic spectra calculated for the three reactions Ca+Ca, Ca+Zr, and Ca+Pb at an incident energy of 1320 MeV. These three reactions are calculated for the respective grazing trajectories defined by a distance of closest approach $d=1.3\ (A_p^{1/3}+A_T^{1/3})$. In Fig. 9 one can see that the excitation of multiphonon structures built with $2\hbar\omega$ giant resonances is a general property of heavy ion reactions. However it appears that these structures are more pronounced in the case of lighter target nuclei.

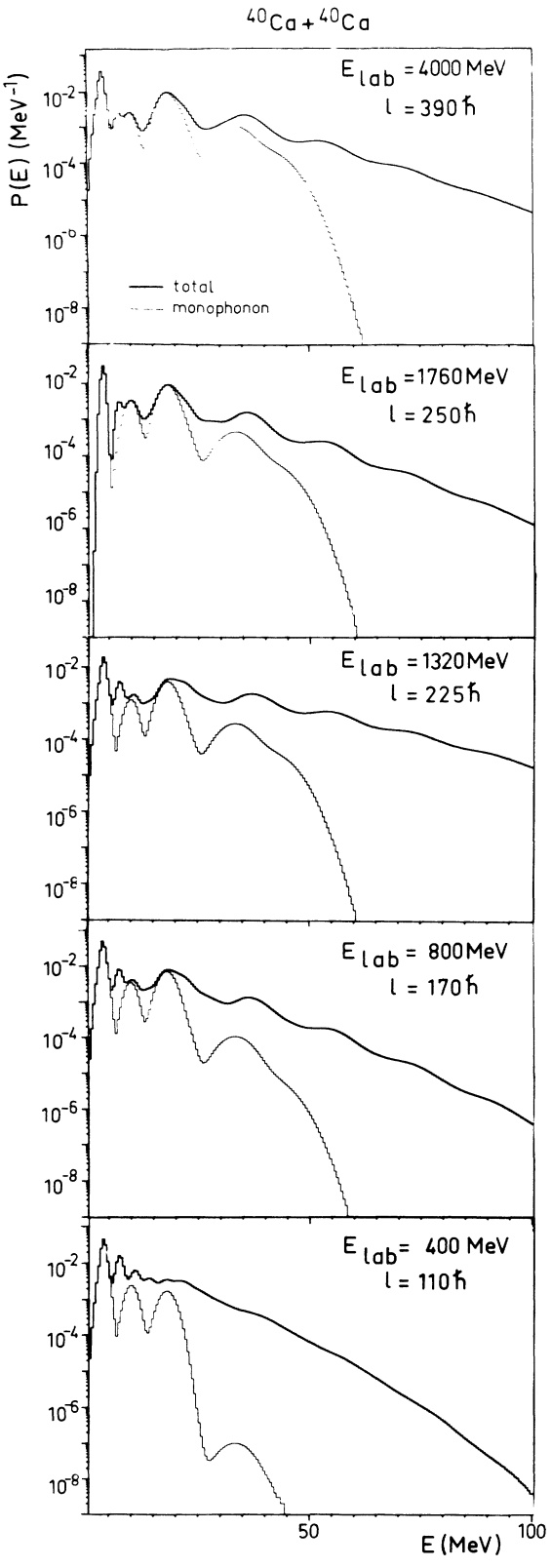

FIG. 8. Inelastic excitation probabilities for the $^{40}Ca+^{40}Ca$ reaction at a distance of closest approach $d=9$ fm for five different incident energies. Thick lines are total probabilities and thin lines represent the monophonon excitations.

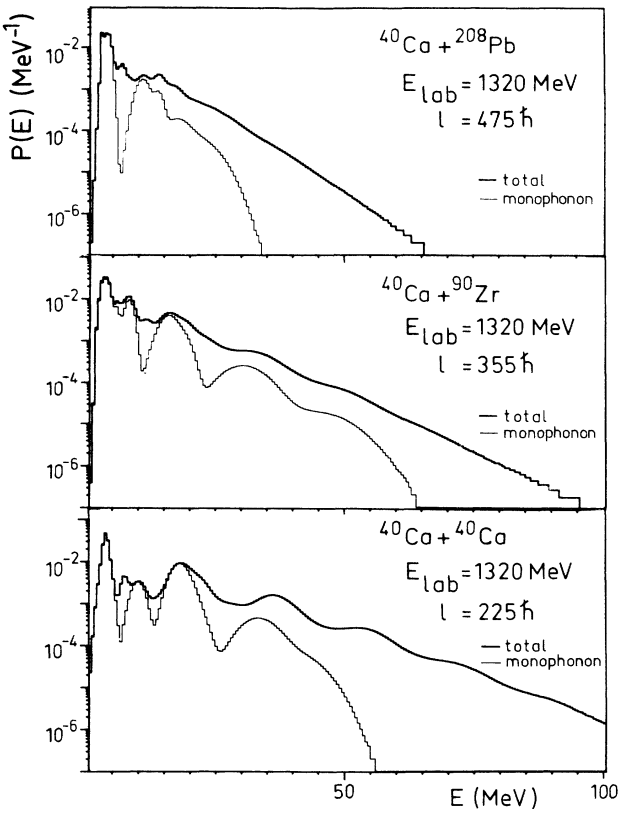

FIG. 9. Inelastic excitation probabilities for the three reactions studied at $E_{lab}=33$ MeV/nucleon and impact parameters slightly inside the grazing. Thick lines are total probabilities and thin lines monophonon.

D. Influence of low-lying states and nonlinear effects

The explanation of the absence of multiphonon structures at low incident energies or for heavy targets can be found on Fig. 10 which displays the mean number of excited phonons for the low lying 3^- state and the giant quadrupole resonance as a function of incident energy for the three considered reactions. In Fig. 10 one should note that the 3^- excitation dominates at low incident energy and for heavy targets. This strong excitation of low-lying states washes out the multiphonon structures built on giant resonances because almost all the excited multiphonon states will contain a contribution of low-lying 3^- excitation. However, the present calculation is a first-order approximation in the sense that the recoupling of low lying states to giant resonances is not taken into account. This is illustrated in Fig. 11: only the linear coupling (1) is included in our calculation and all higher terms such as quadratic terms (2) and (3) are neglected. The influence of the nonlinear coupling between phonons (3) was tested in a previous calculation[22,23] for the Ca+Ca case and it was shown that it induces a depopulation of low lying states and a strong enhancement of the excitation of the giant resonances. This makes both the giant resonance and the multiphonon structures observable in the calculated inelastic cross section. A complete calculation of these higher-order terms will be discussed

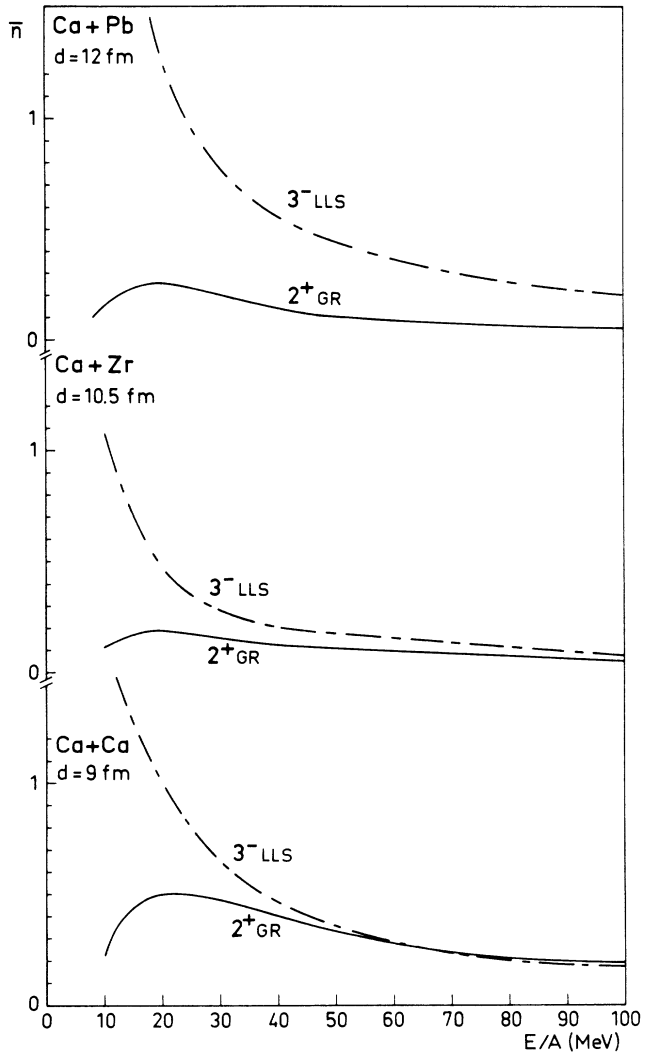

FIG. 10. Mean numbers of excited phonons for the low lying 3^- and giant 2^+ states in the three reactions studied as a function of incident energy. The calculations are performed for the distances of closest approach indicated which correspond to impact parameters slightly smaller than the grazing.

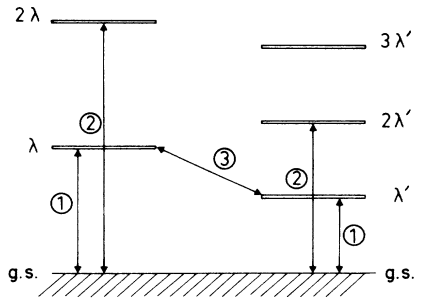

FIG. 11. Schematic diagram of linear and quadratic couplings. Only the linear coupling (1) is taken into account in the calculations presented. The quadratic terms of type (3) will be important whenever a low lying state is strongly excited.

in a forthcoming publication.[28] It is already clear that the effects of such terms will be important for heavy targets because of the strong difference between the excitation of low lying states and giant resonances.

E. Cross section and absorption

In this model the classical cross section is related to the $P(E,\theta)$ function through the formula

$$\frac{d^2\sigma}{dE\,d\Omega}(E,\theta)=\sum_{b(\theta)}\frac{b(\theta)\,|db/d\theta|}{\sin(\theta)}P(E,\theta)T_{\rm tra}(b(\theta))\ , \tag{11}$$

where $b(\theta)$ is the classical deflection function and where the sum runs over all impact parameters b leading to the deflection angle θ. $T_{\rm tra}(b(\theta))$ is the transmission coefficient describing the loss of flux in all the channels not explicitly taken into account in the calculation (e.g., transfer reactions). If all these channels are modelized by a simple imaginary potential W the coefficient $T_{\rm tra}$ can be expressed by

$$T_{\rm tra}(b(\theta))=\exp 2i\int_{-\infty}^{+\infty}\frac{W(R(t))dt}{\hbar}\ . \tag{12}$$

It is interesting to note that the multiphonon excitations are also related to an absorption in the elastic channel. Indeed the flux which remains in the elastic channel is equal to

$$T_{\rm ine}(b(\theta))=\mathcal{N}=\exp\left[-\int N(E,l)dE\right]\ . \tag{13}$$

The function $T_{\rm ine}(b(\theta))$ is shown in Fig. 3(e) for the three reactions at 1320 MeV.

In order to compute the cross section (11) assumptions for W (or $T_{\rm tra}$) must be performed. The simplest assumption is to take $T_{\rm tra}=1$ which will give an upper limit to the cross section $d\sigma/d\Omega\,dE=N_1P(E,\theta)$. The coefficients N_1 associated with the $P(E,\theta)$ functions presented on Fig. 9 are given in Table III. A better approximation is to take $T_{\rm tra}\approx T_{\rm ine}$,[29] which means that the inelastic excitation exhausts roughly one-half of the total absorption. It is shown in Ref. 29 that this is a rather good approximation. The corresponding normalization coefficients N_T $[d\sigma/d\Omega\,dE=N_TP(E,\theta)]$ are given in Table III. The obtained cross sections are in reasonable agreement with the experimental values.[10]

IV. CONCLUSION

The inelastic excitation probabilities for several heavy ion reactions have been calculated and the corresponding inelastic cross sections estimated using a semiclassical model. The trajectories have been treated classically while the nuclear excitations were described microscopi-

TABLE III. Cross-section estimates corresponding to the three spectra of Fig. 9. N_1 gives an upper cross-section limit and N_T takes absorption into account (see text).

E/A (MeV)	Reaction	$l(\hbar)$	θ	N_1 (mb/sr)	N_T (mb/sr)
1320	$^{40}Ca+^{208}Pb$	475	8.5	27	1.9
	$^{40}Ca+^{90}Zr$	355	5.5	48	12.1
	$^{40}Ca+^{40}Ca$	225	3.7	46	23.2

cally using the RPA. The response function thus included both low lying excitations and giant resonances. These RPA states were excited by the nuclear and Coulomb fields of the other partner.

The most remarkable result is that in most cases the excitation of $2\hbar\omega$ giant resonances is large enough to induce structures in the energy spectra due to multiphonon states built with these resonances. The excitation energies, the widths and the cross sections of these multiphonon states are compatible with those of the experimentally observed structures. At low incident energy ($E<10$ MeV/nucleon) and for heavy targets the excitation of the low lying 3^- states is important and washes out most of the structures. However it was shown[22,23] that the inclusion of the coupling between the low lying states and the giant resonances enhances the excitation of the latter and restores the structures in the inelastic spectra.
tra.

The present work shows that the excitation of multiphonon states should contribute with non-negligeable cross section to the inelastic spectra induced by intermediate energy heavy ions. Such multiphonon states built mainly with $2\hbar\omega$ giant resonances could provide a convincing interpretation of the broad regularly spaced structures observed experimentally over a wide range of measured systems.[10]

ACKNOWLEDGMENTS

We wish to thank D. Gogny and J. Dechargé for allowing us to use the results of their RPA calculations. Stimulating discussions with Maria Victoria Andres Martin, F. Catara, H. Flocard, Nimet Frascaria, N. V. Giai, E. Lanza, J. C. Roynette, D. Vautherin, M. Veneroni, and Nicole Vinh Mau are gratefully acknowledged. Division de Physique Théorique is a Laboratoire associé au Centre National de la Recherche Scientifique.

APPENDIX: DOPPLER BROADENING

Consider the two step reaction:

$$1+2\rightarrow 1^*+2\rightarrow 1+\gamma+2\ , \tag{A1}$$

where nucleus 1 is excited and subsequently decays by emission which contributes to the cross section of the inclusive inelastic reaction. In the center of mass (c.m.) of the reaction (A1) the energy of particle 1 after reaction reads as

$$E_1^{\text{c.m.}}=\frac{(P_{1^*}^{\text{c.m.}})^2}{2M_1}+\frac{(\tilde{P}_\gamma)^2}{2M_1}-\frac{2\tilde{P}_\gamma P_{1^*}^{\text{c.m.}}\cos\tilde{\theta}}{2M_1}\ , \tag{A2}$$

where $P_{1^*}^{\text{c.m.}}$ is the impulsion modulus of 1^* in c.m. while $\tilde{P}_\gamma$ and $\tilde{\theta}$ are the modulus and the azimuthal angle of the impulsion of the γ ray in the rest frame of particle 1^* with the z axis cligned on the $\mathbf{p}_{1^*}$ direction. Thus the apparent excitation energy of reaction (A1) can be estimated through the formula

$$E^*=E_{\text{tot}}^{\text{c.m.}}-\frac{M_1+M_2}{M_2}E_1^{\text{c.m.}}=E_1^*-\frac{\Gamma}{2}\cos\tilde{\theta}\ , \tag{A3}$$

where $E_{\text{tot}}^{\text{c.m.}}$ is the total entrance channel center of mass kinetic energy and E_1^* the excitation energy of nucleus 1 in the first step of reaction (A1). In formula (A3) the Doppler broadening Γ is given by

$$\Gamma=2\left[\frac{2E_{\text{lab}}}{A_1mc^2}\right]^{1/2}E_1^*\ , \tag{A4}$$

where A_1 is the mass number of particle 1 (i.e., the projectile) while m is the nucleon mass. For example, for a ^{40}Ca projectile at an excitation energy of $E_1^*=4$ MeV, Eq. (A4) yields $\Gamma=1.2$ MeV at 10 MeV/nucleon, $\Gamma=2.5$ MeV at 44 MeV/nucleon, and $\Gamma=3.7$ MeV at 100 MeV/nucleon.

[1]M. Buenerd *et al.*, Phys. Rev. Lett. **40**, 1482 (1978).
[2]P. Doll *et al.*, Phys. Rev. Lett. **42**, 366 (1979).
[3]Ph. Chomaz, J. Phys. C **47**, 155 (1986).
[4]F. E. Bertrand, Nucl. Phys. **A354**, 129c (1981).
[5]R. A. Broglia *et al.*, Phys. Lett. **61B**, 113 (1976).
[6]T. P. Sjoreen *et al.*, Phys. Rev. C **29**, 29 (1984).
[7]N. Frascaria *et al.*, Phys. Rev. Lett. **39**, 918 (1977).
[8]S. Fortier *et al.*, Phys. Rev. C **36**, 1830 (1987).
[9]Ph. Chomaz, Ph. D. thesis, Institut de Physique Nucléaire, Orsay, France, 1984; Ph. Chomaz *et al.*, Z. Phys. A **318**, 41 (1984).
[10]N. Frascaria *et al.*, Nucl. Phys. **A474**, 253 (1987).
[11]H. Tricoire, C. Marty, and D. Vautherin, Phys. Lett. **100B**, 109 (1981).
[12]Nguyen van Giai, Phys. Lett. **105B**, 11 (1981).
[13]S. A. Fayans, V. V. Palichnick, and N. I. Pyatov, Z. Phys. A **308**, 145 (1982).
[14]J. Decharge *et al.*, Phys. Rev. Lett. **49**, 982 (1982).
[15]H. Flocard and M. Weiss, Phys. Lett. **105B**, 16 (1981).
[16]Ph. Chomaz and D. Vautherin, Phys. Lett. **139B**, 244 (1984).
[17]Ph. Chomaz *et al.*, Z. Phys. A **319**, 167 (1984).
[18]G. Pollarolo *et al.*, Nucl. Phys. **A451**, 122 (1986).

[19]Ph. Chomaz, N. V. Giai, and D. Vautherin, Nucl. Phys. A (to be published).
[20]R. A. Broglia *et al.*, Phys. Lett. **89B**, 22 (1979).
[21]R. A. Broglia, Ch. Dasso, and A. Winther, Proceedings of the International School of Physics "Enrico Fermi," Course LXXVII, Varenna, 1981, edited by R. A. Broglia, C. H. Dasso, and R. Ricci (North-Holland, Amsterdam, 1981), p. 327; R. A. Broglia, C. H. Dasso, and H. Eslensen, *Progress in Particle and Nuclear Physics* (Pergamon, New York, 1980), Vol. 4, p. 345.
[22]F. Catara and U. Lombardo, Nucl. Phys. **A455**, 158 (1986).
[23]F. Catara, Ph. Chomaz, and A. Vitturi, Nucl. Phys. **A471**, 661 (1987).
[24]Ph. Chomaz and D. Vautherin, Phys. Lett. B **177**, 9 (1986).
[25]J. Decharge and L. Sips, Nucl. Phys. **A407**, 1 (1983).
[26]G. R. Satchler, Phys. Lett. **55B**, 167 (1975); **59B**, 12 (1975).
[27]Y. Blumenfeld *et al.*, Nucl. Phys. **A445**, 151 (1985).
[28]Ph. Chomaz and F. Catara (unpublished).
[29]N. Vinh Mau, Nucl. Phys. **A457**, 413 (1986).